RSC Advances

ROYAL SOCIETY OF CHEMISTRY

www.rsc.org/advances

Theoretical analyses of the fluorescence lifetimes of the D-amino acid oxidase–benzoate complex dimer from porcine kidney: Molecular dynamics simulation and photoinduced electron transfer

Arthit Nueangaudom,[a] Kiattisak Lugsanangarm,[a] Somsak Pianwanit,[a] Sirirat Kokpol,[a,*] Nadtanet Nunthaboot,[b] Fumio Tanaka,[a,c,*] Seiji Taniguchi[c] and Haik Chosrowjan[c]

[a] *Department of Chemistry, Faculty of Science, Chulalongkorn University, 254 Phayathai Road, Bangkok 10330, Thailand. E-mail: Somsak.t@chula.ac.th*

[b] *Department of Chemistry, Faculty of Science, Mahasarakham University, Mahasarakham 44150, Thailand*

[c] *Division of Laser Biochemistry, Institute for Laser Technology, Utsubo-Honmachi, 1-8-4, Nishiku, Osaka 550-0004, Japan. E-mail: fumio.tanaka@yahoo.com*

Abstract

The mechanism of photoinduced electron transfer (ET) from benzoate (Bz) and aromatic amino acids to the excited isoalloxazine (Iso*) in the D-amino acid oxidase-benzoate complex (DAOB) dimer from porcine kidney was studied using molecular dynamics simulation (MDS) and an electron transfer theory, and compared with that in the DAOB monomer. DAOB dimer displayed two fluorescent lifetime components of 0.85 ps and 4.8 ps, as reported. The ET parameters contained in the Kakitani and Mataga (KM) model were determined so as to reproduce these lifetimes with MDS atomic coordinates. The Bz-isoalloxazine (Iso) distances were 0.66 nm in subunit A (Sub A), 0.68 nm in subunit B (Sub B) and 0.61 nm in the monomer. The fluorescent lifetimes of 4.8 ps and 0.85 ps were found to originate from Sub A and Sub B, respectively. In Sub A, Tyr228 was the fastest ET donor followed by Bz and Tyr55, while Bz was followed by Tyr228 and Tyr314 in Sub B. The ET rate from Bz was fastest in Sub B, followed by that in Sub A and the DAOB monomer. The static dielectric constants obtained near Iso were 2.4-2.6 in the DAOB dimer and monomer and 5.8-5.9 in holo D-amino oxidase (DAAO). The different dielectric constants could account for experimental fluorescence peak observed for DAOB (524 nm) and DAAO (530 nm). Logarithmic ET rates decreased linearly with the donor-acceptor distance expressed by both center to center distance (Rc) and edge to edge distance (Re) in Sub A and Sub B of DAOB dimer and monomer, which reveals that the conventional Dutton ruler holds in the ET processes in DAOB. The logarithmic ET rates were decomposed into the electronic coupling (*EC*), square root (*SQ*) and exponential (*GTRAM*) terms. It was found that both the *EC* term and the *GTRAM* term also decreased linearly with Rc.

The sum of the slopes in the *EC* and *GTRAM vs*. Rc plots coincided with the slopes in the logarithmic ET rate vs Rc functions, suggesting that the *GTRAM* term makes a significant contribution to the linear relations between logarithmic ET rate and Rc.

I. Introduction

D-amino acid oxidase (DAAO) from porcine kidney contains flavin adenine dinucleotide (FAD) as a cofactor,[1,2] and exists in a wide range of species from yeasts to human.[3–5] Its function is to oxidize D-amino acids to the corresponding imino acids, producing ammonia and hydrogen peroxide. Recently, mammalian DAAO has been demonstrated to be involved in D-serine metabolism in the brain and to regulate glutamatergic neurotransmission.[6,7] Various novel inhibitors to human DAAO have been found by means of *in silico* screening.[8]

DAAO from porcine kidney exists in a monomer (Mw 39 kDa)-dimer equilibrium state at relatively low concentrations,[9–12] and may be in a dimer-tetramer equilibrium at higher concentrations.[13–15] The crystal structures of the DAAO-benzoate (Bz) complex (DAOB) dimer have been determined.[16,17] Each subunit of the DAOB dimer contains Iso as the ET acceptor, and one Bz, 10 Trp and 14 Tyr residues as potential ET donors.

The fluorescence of flavins in many flavoproteins is strongly quenched, which is ascribed to photoinduced electron transfer (ET) from tryptophans (Trp) and/or tyrosines (Tyr) to the excited isoalloxazine (Iso*).[18–20] Fluorescence dynamics of flavoproteins have been worked in the picoseconds domain by Visser et al,[21,22] by means of photon-counting method. Ultrafast fluorescence dynamics of some flavoproteins in the time

domain of femtoseconds to picoseconds have been studied by means of fluorescence up-conversion,[23–27] and theoretically by molecular dynamics simulation (MDS) and an electron transfer theory[28–32] using the available protein structures.[16,17]

The structural basis for the temperature-induced transition of the DAAO monomer has been analyzed by MDS with the Kakitani and Mataga (KM) equation based ET theory.[33] The conformational change was characterized with the ET rates from Tyr224, Tyr228 and Tyr314 to the Iso*. The fluorescence lifetimes of flavin in DAAO and DAOB monomer have been reported to be 160 and 60 ps, respectively, with the decreased lifetime upon the binding of Bz to DAAO being ascribed to the fast ET from Bz to Iso*.[34,35] The fluorescence dynamics of the DAOB dimer has been reported by means of the up-conversion,[23] whilst it was recently reported that the DAAO dimer displays non-equivalent conformations between the two subunits.[36] In the present work we have demonstrated by means of MDS structures and KM-theory based ET analysis that not only the structure of the DAOB dimer is quite different from the DAOB monomer, but also the conformations of subunit A (Sub A) and Sub B of the DAOB dimer are non-equivalent.

II. Methods of analyses

MDS calculation

The starting structure of DAOB was obtained from the X-ray structure in the protein data bank (PDB code: 1VE9).[16] The MDS and all calculations were performed using the AMBER 10 suite of programs.[37] The parm99 force field[38] was used to describe the protein atoms the general Amber force field with the restrained electrostatic

potential[37] charges was used for the FAD and Bz, and all missing hydrogen atoms of the protein were added using the LEaP module.[39] The simulated systems were subsequently solvated with a cubic box of 27,390 TIP3P water molecules, and the electroneutrality of the system was attained by adding 10 sodium counter-ions. The systems were set up under the isobaric-isothermal ensemble with a constant pressure (1 atm) and temperature (293 K). Electrostatic interactions were corrected by the Particle Mesh Ewald method.[40] The SHAKE algorithm[41] was used to constrain all bonds involving hydrogen atoms. All MDS based calculations were performed with a time steps of 2 fs and a non-bond-interaction cut off radius of 10 Å. The coordinates of the MDS snapshots were collected every 0.1 ps. Equilibrium, attained after 20 ns of the MDS calculation, was ascertained by monitoring the global root mean square deviation (RMSD). The calculation was then continued for up to a further 30 ns, and the last 5 ns data were used for the analyses.

ET rates from Trp and Tyr

The original Marcus theory[42,43] has been modified in various ways.[44–48] In the present analysis, KM theory[47] was used, because it is applicable for both non-adiabatic ET processes and adiabatic ET processes, and has been found to give satisfactory results for both static,[27,,33,35,36] and dynamic ET analyses.[28–32] When the donor is Trp or Tyr, the ET rate described by the KM theory is expressed by eqn (1).

$$k_{ET}^{j} = \frac{\nu_0^q}{1+\exp\left\{\beta^q (R_j - R_0^q)\right\}} \sqrt{\frac{k_B T}{4\pi\lambda_S^{qj}}} \exp\left[-\frac{\left\{\Delta G_q^0 - e^2/\varepsilon_0^p R_j + \lambda_S^{qj} + ES_j(k)\right\}^2}{4\lambda_S^{qj} k_B T} \right] \quad (1)$$

Here k_{ET}^{j} is the ET rate from a donor j (j = 1–10 for Trp, j = 11–24 for Tyr) to the photoexcited Iso*, and q denotes Trp or Tyr. ν_0^q is an adiabatic frequency, β^q is the

ET process coefficient. R_j and R_0^q is the donor *j*–Iso distance and its critical distance for the ET process, respectively. R_j is expressed as a center-to-center (Rc) distance rather than as an edge-to-edge (Re) distance.[26–31,46,47] The ET process is adiabatic when $R_j < R_0^q$, and non-adiabatic when $R_j > R_0^q$. The terms k_B and e are the Boltzmann constant and electron charge, respectively. *T* is the temperature (K), and here was fixed at 293 K (20 °C). The term $-e^2 / \varepsilon_0^p R_j$ in eqn (1) is the electrostatic energy (ES) between the Iso anion and a donor cation (ESDA). The static dielectric constant ε_0^p is described below. ES_j is a net the ES energy (NetES) between the donor *j* cation and other ionic groups, which is also described below. Each subunit of the DAOB dimer contains one Bz, 10 Trp and 14 Tyr residues as potential donors. The ET rates from all of these donors to Iso* were taken into account for the analysis.

λ_S^{qj} is the solvent reorganization energy[42,43] of the ET donor *q* and *j*, and is expressed as eqn (2);

$$\lambda_S^{qj} = e^2 \left(\frac{1}{2a_{Iso}} + \frac{1}{2a_q} - \frac{1}{R_j} \right) \left(\frac{1}{\varepsilon_\infty} - \frac{1}{\varepsilon_0^p} \right), \qquad (2)$$

where a_{Iso} and a_q are the radii of isoalloxazine (Iso) and one of Trp or Tyr, with these reactants being assumed to be spherical, and ε_∞ and ε_0^p are the optical and static dielectric constants in the domain among Iso and donors, respectively. In this study, the optical dielectric constant was set as 2.0. In eqns (1) and (2) it was assumed that $\varepsilon_0^p = \varepsilon_0^{DA}$ for Bz, Tyr55 and Tyr228 in Sub A, and $\varepsilon_0^p = \varepsilon_0^{DB}$ for Bz and Tyr228 in Sub B, where the mean Rc values were shorter than 1 nm (see Table 1), and $\varepsilon_0^p = \varepsilon_0$ for both

Sub A and Sub B in the other donors.[36] The previously determined values for the radii of Iso (a_{Iso}), Trp (a_{Trp}) and Tyr (a_{Tyr}) of 0.224, 0.196 and 0.173 nm, respectively, [28–33] were used.

The standard free energy change was expressed with the ionization potential of the ET donor (E_{IP}^{q}) as eqn (3);

$$\Delta G_q^0 = E_{IP}^q - G_{Isop}^0 , \quad (3)$$

where G_{Isop}^0 is standard free energy related to the electron affinity of Iso*. $G_{Isop}^0 = G_{IsoA}^0$ for Sub A, and $G_{Isop}^0 = G_{IsoB}^0$ for Sub B. The values of E_{IP}^q for Trp and Tyr were 7.2 eV and 8.0 eV, respectively.[49]

ET rate from Bz

When the donor is Bz, the ET rate may be expressed by eqn (4);

$$k_{ET}^{Bz} = \frac{\nu_0^{Bz}}{1+\exp\left\{\beta^{Bz}(R_{Bz}-R_0^{Bz})\right\}}\sqrt{\frac{k_B T}{4\pi\lambda_S^{Bz}}}\exp\left[-\frac{\left\{\Delta G_{Bz}^0 + E_{Iso}^{Bz} + \lambda_S^{Bz} + ES_{Bz}\right\}^2}{4\lambda_S^{Bz} k_B T}\right], \quad (4)$$

where ν_0^{Bz}, β^{Bz} and R_0^{Bz} are the adiabatic frequency, ET process coefficient and critical ET distance of Bz, respectively. In this case the solvent reorganization energy is represented as eqn (5);

$$\lambda_S^{Bz} = e^2\left(\frac{1}{2a_{Iso}} + \frac{1}{2a_{Bz}} - \frac{1}{R_{Bz}}\right)\left(\frac{1}{\varepsilon_\infty} - \frac{1}{\varepsilon_0^p}\right), \quad (5)$$

where a_{Bz} was 0.108 nm.[35] R_{Bz} is the Rc distance between Iso and Bz. The ES energies between the photoproducts and ionic groups (ES_{Bz}), and between the Iso anion and a neutral radical of Bz (E_{Iso}^{Bz}) are described below. The standard free energy gap (ΔG_{Bz}^0) is given by eqn (6);

$$\Delta G^0_{Bz} = E^{Bz}_{IP} - G^0_{Isop}, \quad (6)$$

where E^{Bz}_{IP} denotes the ionization potential of Bz, which was previously determined to be 7.25 eV.[35]

Electrostatic energy in the DAOB dimer

Protein systems contain many charged/polar moieties which may influence the ET rate. Ionic groups in each subunit of DAOB are the negatively charged pyrophosphate (-2) in FAD, Bz (-1), 22 Glu (-1) and 13 Asp (-1), plus the positively charged 12 Lys (+1) and 21 Arg (+1) residues, resulting in a net charge of -5. In the dimer, the total number of point charges are double that of the monomer and was counterbalanced in the MDS by 10 sodium ions.

When the donor is Trp or Tyr, the ES energy between the donor cation $j \geq 1$ and all other ionic groups in the protein is expressed by eqn (7);

$$E(j) = \sum_{i=1}^{44} \frac{C_j C_{Glu}}{\varepsilon_0 R_j (Glu - i)} + \sum_{i=1}^{26} \frac{C_j C_{Asp}}{\varepsilon_0 R_j (Asp - i)}$$

$$+ \sum_{i=1}^{24} \frac{C_j C_{Lys}}{\varepsilon_0 R_j (Lys - i)} + \sum_{i=1}^{42} \frac{C_j C_{Arg}}{\varepsilon_0 R_j (Arg - i)} + \sum_{i=1}^{8} \frac{C_j C_P}{\varepsilon_0 R_j (P - i)}, \quad (7)$$

where j = 1–10 for the Trp cations and 11–24 for the Tyr cations. C_j is the charge of the aromatic ionic species j, that is $+e$ for j = 1–24. C_{Glu} (= - e), C_{Asp} (= - e), C_{Lys} (= + e) and C_{Arg} (= + e) are the charges of the Glu, Asp, Lys and Arg residues, respectively. FAD contains two phosphorus atoms, each of which is bonded to two oxygen atoms with charges. It was assumed that the charge of each oxygen atom (C_P) is -0.5e, and then the total charge at the four phosphate atoms is -2e. We also assumed that these groups are

all in an ionic state in solution. The pK_a values of the charged amino acids (Glu, Asp, Lys, Arg and His) in water are 4.3, 3.9, 10.5, 12.5 and 6.0, respectively. Although these pK_a values may be slightly modified in proteins, they are still likely to be fully ionized in the 17 mM pyrophosphate buffer (pH 8.3) that all the measurements were performed.[23] The positions of Glu and Asp were expressed by the coordinates of the center of the two O atoms of the side chain, Lys by the coordinates of N atom of the side chain and Arg by the coordinates of the center between two edge N atoms of the side chain. The distances between the aromatic ionic species j and the i^{th} Glu (i = 1–44) are denoted as $R_j(Glu-i)$, whilst the distances between the aromatic ionic species j and the i^{th} Asp (i = 1–26) are denoted as $R_j(Asp-i)$, and so on for each ionic group. These distances were evaluated as the average distances over all atoms in the aromatic donors.

The ES energy between the Iso anion and the ionic groups was obtained by eqn (8);

$$E_{Iso} = \sum_{i=1}^{44} \frac{C_{Iso}C_{Glu}}{\varepsilon_0 R_{Iso}(Glu-i)} + \sum_{i=1}^{26} \frac{C_{Iso}C_{Asp}}{\varepsilon_0 R_{Iso}(Asp-i)}$$

$$+\sum_{i=1}^{24} \frac{C_{Iso}C_{Lys}}{\varepsilon_0 R_{Iso}(Lys-i)} + \sum_{i=1}^{42} \frac{C_{Iso}C_{Arg}}{\varepsilon_0 R_{Iso}(Arg-i)} + \sum_{i=1}^{8} \frac{C_{Iso}C_{P}}{\varepsilon_0 R_{Iso}(P-i)}, \quad (8)$$

where C_{Iso} = -e. The distances between Iso and the i^{th} Glu (i = 1–44) are denoted as $R_{Iso}(Glu-i)$, whilst the distances between Iso and the i^{th} Asp (i = 1–26) are denoted as $R_{Iso}(Asp-i)$, and so on for all the aromatic amino acids.

ES_j in eqn (1) was expressed as eqn (9);

$$ES_j = E_{Iso} + E(j), \quad (9)$$

Where j is from 1–24, and represents the j^{th} ET donor, as described above.

When the donor is Bz, the ES energies have to be considered separately from Trp and Tyr, since the photoproduct of Bz is neutral, which is in contrast to that for Trp and Tyr which are cations. In the point charge approximate utilized above, the ES energies between the neutral radical of Bz produced by ET and all other ionic species totals to zero. Accordingly, these ES energies were calculated using the charge densities of atoms in neutral Bz by eqn (10);

$$E_{Bz} = \frac{1}{N_{Bz}} \sum_{l=1}^{N_{Bz}} [\sum_{i=1}^{44} \frac{D_{Bz}^{l} C_{Glu}}{\varepsilon_0 R_{Iso}(Glu-i)} + \sum_{i=1}^{26} \frac{D_{Bz}^{l} C_{Asp}}{\varepsilon_0 R_{Iso}(Asp-i)}$$

$$+ \sum_{i=1}^{24} \frac{D_{Bz}^{l} C_{Lys}}{\varepsilon_0 R_{Iso}(Lys-i)} + \sum_{i=1}^{42} \frac{D_{Bz}^{l} C_{Arg}}{\varepsilon_0 R_{Iso}(Arg-i)} + \sum_{i=1}^{8} \frac{D_{Bz}^{l} C_{P}}{\varepsilon_0 R_{Iso}(P-i)}], \quad (10)$$

where D_{Bz}^{l} denotes the charge density of the neutral radical of Bz at atom *l* and N_{Bz} is the number of atoms in Bz and is equal to 14. $\sum_{l=1}^{N_{Bz}} D_{Bz}^{l} = 0$ holds. The ES energies between the Iso anion and the neutral Bz were also calculated from their respective charge densities using eqn (11),

$$E_{Iso}^{Bz} = \frac{e^2}{N_{Iso} N_{Bz}} \sum_{i=1}^{N_{Iso}} \sum_{j=1}^{N_{Bz}} \frac{D_{Iso}^{i} D_{Bz}^{j}}{\varepsilon_0^{p} R_i^{j}}. \quad (11)$$

The charge density of atom *i* in the Iso anion is denoted as D_{Iso}^{i}. $\sum_{i=1}^{N_{Iso}} D_{Iso}^{i} = -1$ holds. N_{Iso} is number of atoms of lumiflavin and is equal to 31. D_{Bz}^{l} and D_{Iso}^{i} were used as obtained and reported previously.[35] The NetES energy for Bz is given by eqn (12),

$$ES_{Bz} = E_{Bz} + E_{Iso}^{Bz}. \quad (12)$$

Determination of the ET parameters

The fluorescence spectrum of the DAOB dimer showed an emission peak at 524 nm (Fig. S1, Supporting Information). The fluorescence decays of the DAOB dimer with two-exponential decay functions have been reported previously by Mataga *et al.*[23] and the decay functions at the emission wavelength (λ) are expressed by eqn (13);

$$F(\lambda t) = \alpha_1(\lambda)\exp\{-t/\tau_1(\lambda)\} + \alpha_2(\lambda)\exp\{-t/\tau_2(\lambda)\}, \quad (13)$$

where $\tau_1(\lambda)$ and $\tau_2(\lambda)$ are the emission wavelength-dependent fluorescence lifetimes of components 1 and 2, respectively, $\alpha_1(\lambda)$ and $\alpha_2(\lambda)$ are their emission wavelength-dependent fractions and $\alpha_1(\lambda)$ + $\alpha_2(\lambda)$ = 1. The decay parameters are listed in Table S1 (SI).

Some of the ET parameters contained in eqns (1)–(11) have been reported previously,[28-33, 35,36] whilst the parameters used in the present work are listed in Table 2. First we tried to reproduce the experimental lifetimes with the previously obtained ET parameters, but the agreements between the calculated and observed lifetimes were not satisfactory (not shown). Accordingly, in the present ET analysis G^0_{IsoA}, G^0_{IsoB}, R_0^{Bz}, ε_0^{DA}, and ε_0^{DB} were chosen as adjustable parameters to obtain a best-fit between the observed and calculated lifetimes. G^0_{IsoA} and G^0_{IsoB} are the free energies related to electron affinities of Iso* in Sub A and Sub B, respectively, while ε_0^{DA} and ε_0^{DB} are the static dielectric constants between Iso and the donors (Bz, Tyr55 and Tyr228) in Sub A and between Iso and the donors (Bz and Tyr228) in Sub B, respectively (see below eqn (2)). R_0^{Bz} is the critical ET distance for Bz in eqn (4). The other ET parameters are common to both subunits. The unknown ET parameters were determined by two

methods, where the minimum chi-squared values (χ_1^2 or χ_2^2) were derived from eqns (14) and (15) in methods 1 and 2, respectively:

$$\chi_1^2 = \frac{\left(\tau_{obs}^1 - \tau_{calc}^A\right)^2}{\tau_{calc}^A} + \frac{\left(\tau_{obs}^2 - \tau_{calc}^B\right)^2}{\tau_{calc}^B}, \quad (14)$$

$$\chi_2^2 = \frac{\left(\tau_{obs}^1 - \tau_{calc}^B\right)^2}{\tau_{calc}^B} + \frac{\left(\tau_{obs}^2 - \tau_{calc}^A\right)^2}{\tau_{calc}^A}. \quad (15)$$

The observed lifetimes, τ_{obs}^1 (0.848 ps) and τ_{obs}^2 (4.77 ps), are the mean lifetimes of $\tau_1(\lambda)$ and $\tau_2(\lambda)$ in eqn (13), respectively, over 10 emission wavelengths (λ). In method 1 (χ_1^2) it was assumed that the fluorescent component with τ_{obs}^1 and τ_{obs}^2 were from Sub A and Sub B, respectively, whilst in method 2 (χ_2^2) it was assumed that the fluorescent component with τ_{obs}^1 and τ_{obs}^2 were from Sub B and Sub A, respectively. The obtained values of χ_1^2 and χ_2^2 were then compared to determine the likely ET mechanism in the DAOB dimer.

Molecular orbital study of charge densities of Iso and hydrogen bonding amino acids.

The charge densities were obtained by a semi-empirical MO method with the software package of MOPAC2009. The keywords, EF (geometrical optimization), PRECISE (accurate calculation), PM6 (semi-empirical Hamiltonians), XYZ (geometry expressed by (x,y,z) coordinates), GEO-OK (neglect check on abnormal access of atoms), EPS (dielectric constant for COSMO solvation energy) were used. The details of these keywords are found on the website: http://openmopac.net. In addition to these keywords, the keyword EXCITED was used for Iso*. The values of EPS were 2.6 both for Sub A

and Sub B, because ε_0^{DA} and ε_0^{DB} were close to 2.6 (see Table 3). Sub A formed hydrogen bondings (H-bond) with Ala49, Leu51 and Thr317 in Sub A, and with Ala49 and Leu51 in Sub B. The charge densities of Iso and Iso* were calculated with and without H-bond clusters.

III. Results

Comparisons between MDS snapshot and crystal structure and between the two subunits in the DAOB dimer.

Fig. 1 shows the MDS snapshot of the two subunits of the DAOB dimer superimposed on the crystal structure. In Fig 1A, the crystal structure of Sub A was superimposed on that of Sub B and in Figure 1B MDS snapshot of Sub A was superimposed on that of Sub B. In crystal the local structures of Sub A and Sub B[16] are almost equivalent. However, in the MDS snapshots the both structures displayed considerable difference between Sub A and Sub B, especially in the aromatic amino acids of Tyr224, Tyr55 and Tyr314 among the chromophores were quite different between Sub A and Sub B.. The structures were compared between the crystal and MDS for Sub A in Fig. 1C, and for Sub B in Fig, 1D. It is obvious that the crystal and MDS structures are quite different both in Sub A and Sub B, not only near Iso binding site, but also in the entire protein (Fig. 1E). This may be ascribed to the presence of freely mobile water molecules near the protein in MDS snapshots.

Time-evolutions of the Rc between the potential donors and Iso are shown in Fig. S2 (Supporting Information), whilst the Rc distributions of potential ET donors

including Bz are shown in Fig. 2, where large differences were evident in the Rc distributions of Tyr55 and Trp185 between Sub A and Sub B, whilst Tyr144 and Tyr224 were present only in Sub A or Sub B, respectively. The mean Rc values between Iso and these donors, derived from 5000 snapshots with 1 ps time intervals, are listed in Table 1. The Rc distance for Bz was shortest among the monomer and the dimer subunits, and slightly shorter in Sub A than Sub B. The Rc values were higher by 0.05 and 0.07 nm respectively in Sub A and Sub B compared to that in the monomer. Within the dimer subunits, the Rc for Trp185 was shorter in Sub A (1.10 nm) than in Sub B (1.31 nm), while it was 1.39 nm in the monomer. The Rc values of Tyr55 were slightly (1.1-fold) smaller in Sub A (0.95 nm) than Sub B (1.05 nm), but much larger in the monomer (1.31 nm) with only that in Sub A being < 1 nm. The Rc values of Tyr228 were similar in Sub A and Sub B (0.96 and 0.99 nm), but markedly smaller in the monomer (0.81 nm) and with all three being shorter than 1 nm. The Rc value for Tyr 224 in sub B (1.04 nm) was closer to that of the monomer (0.97 nm) but was much larger in Sub A (1.32 nm). In contrast, the Rc values for Tyr314 were similar in all three systems. Thus, the protein conformations near Iso were quite different between Sub A and Sub B in the dimer, and in the monomer.

Root of mean square deviation and root of mean square fluctuation

Root of mean square deviation (RMSD) and root of mean square fluctuation (RMSF) were obtained using the AMBER10 software. Time-evolutions of RMSD of the entire protein (Sub A and Sub B), FAD and Bz are shown in Fig. S3 (Supporting Information). The RMSDs of all components attained equilibrium between 25-30 ns of MDS calculations. The RMSF is considered to be a useful index for protein fluctuation, and the RMSF for the amino acid residues is shown in Fig. S4 along with those from the

literature for the DAOB monomer,[35] holoDAAO monomer,[33] and Sub A and Sub B of the holoDAAO dimer[36] for comparison. The mean RMSF values over all the amino acids were small in Sub A and Sub B of the DAOB dimer (0.191 and 0.171, respectively), but much larger in the DAOB monomer (0.522), and in Sub A and Sub B of the holoDAAO dimer (0.347 and 0.344), respectively, and largest in the holoDAAO monomer (0.701). The lowest mean RMSF values were hence found in the DAOB dimer and the highest in the holoDAAO monomer, whilst the mean RMSF value of the DAOB monomer was higher than those of the holoDAAO dimer. It is well known that Bz binding to holoDAAO from porcine kidney greatly stabilizes the protein, and indeed this trait is used in the purification of holoDAAO.[12] It is also recognized that the holoDAAO monomer is the most unstable of the protein species. Thus, the mean RMSD may be related to protein stability in general.

Best-fit ET parameters

In holoDAAO dimer the static dielectric constant (ε_0^{DA}) was introduced between Iso and the donors only when the mean Rc is shorter than 1 nm.[36] This model was also used in the present work (see below eqn (2)). However, in DAOB monomer ε_0^{DA} was introduced for all donors.[33] To compare the ET parameters in the DAOB dimer with those in the DAOB monomer, first the fluorescence lifetime of the DAOB monomer[34] (60 ps) was analyzed with the same model as the present work, introducing ε_0^{DA} only for the donors with the mean Rc shorter than 1 nm. The ET parameters of the monomer obtained with this model are listed in Table S2 (SI). The values of ν_0^{Bz}, β^{Bz} and E_{IP}^{Bz} (ionization potential of the Bz anion) were the same as those previously reported.[35] The obtained value of ε_0 was 5.78, which was similar to that previously reported, but the

values of R_0^{Bz} (0.384 nm) and ε_0^{DA} (2.45) were a little larger (0.116 and 2.22 respectively).[35] The calculated lifetime of the DAOB monomer completely coincided with one of the observed lifetimes (that at 60 ps).[34]

The unknown ET parameters for the DAOB dimer were G_{IsoA}^0, G_{IsoB}^0, ε_0^{DA}, ε_0^{DB}, ε_0 and R_0^{Bz}. These best-fit parameters, obtained with Methods 1 and 2 (see **Determination of the ET parameters** section), are listed in Table 4. The total chi-squared values were 64-fold larger with Method 1 than with Method 2, and so Method 2 seems to be a better method. The best-fit parameters (from Method 2) were G_{IsoA}^0 = 8.42 eV, G_{IsoB}^0 = 8.43 eV, ε_0^{DA} = 2.53, ε_0^{DB} = 2.64 and R_0^{Bz} = 0.462 nm.

ET rates in DAOB dimer.

The ET rates from all Tyr and Trp residues in addition to Bz were obtained with the ET parameters described above. Fig. S5 (Supporting Information) shows the time-evolutions of the logarithmic ET rates of the six fastest donors, including Bz. Fig. 3 shows the distributions of the logarithmic ET rates, with the distributions in the DAOB monomer, obtained with the ET parameters listed in Table S2 (Supporting Information), also shown for comparison. The distributions of logarithmic ET rate in Tyr314 of Sub A displayed a double maxima, and Trp185 displayed a broad shoulder. The distributions for each donor were markedly different between the two subunits and in the monomer. Table 5 lists the mean ET rates over 5000 snapshots with 1 ps time intervals, together with the physical quantities related to ET. In Sub A the fastest rate was from Tyr228, then followed by Bz, Tyr55, Trp185, Tyr314 and Trp52. However, in Sub B the fastest donor was Bz (11.8-fold faster than in Sub A, and 7.62-fold faster than Tyr228 in Sub

A), and then followed by Tyr228, Tyr314, Tyr55, Tyr224 and Trp185. In the monomer, the fastest donor was also Bz and then followed by Tyr228, Tyr224, Tyr314, Tyr55 and Trp185, but the mean ET rates in each case were more than 10-fold slower than in the dimer subunits.

NetES energy

The time-evolutions of NetES energies between the photoproducts and ionic groups in the DAOB dimer are shown in Fig. S6 (Supporting Information), with the distributions of the NetES energies shown in Fig. 4 along with those in the monomer for comparison. The NetES energies in the dimer ranged from -0.5 eV to 0.2 eV, while those in monomer ranged from -0.3 – 1.0 eV. The mean NetES energies are listed in Table 4. Tyr228 had the fastest ET rate and the highest NetES energy in Sub A, but in Sub B whilst Bz had the fastest ET rate, its NetES energy was 1.7 fold lesser than that for Tyr228. Thus, the NetES energy was highest in Tyr228 in both Sub A and Sub B. The lowest NetES energy was found in Trp185 in Sub A (followed by trp314) and in Tyr314 in Sub B (followed by Trp185), whilst the NetES energies of Bz were similar in both subunits. Note that the NetES energies of Tyr314 in Sub A displayed a double maximum at around -0.3 eV and -0.4 eV.

The NetES energy of Bz in the monomer was much higher (11-fold) than those in either subunits of the dimer, and the same trend was noted for all of the other five donors (Table 4). This revealed that in the dimer the NetES energies in each subunit were influenced by those in the other subunit.[34] The mean values of NetES energies in the aromatic amino acids of the monomer were also higher than in the dimer subunits.

The other physical quantities related to ET.

The time-evolution of the ESDA between the Iso anion and donor cation (aromatic amino acids) or neutral radical (Bz) are shown in Fig. S7 (Supporting Information), and the ESDA distributions and mean values are shown in Fig. 5 and Table 4, respectively. The ESDA of the Bz neutral radical in the dimer fluctuated around zero (slightly negative) with appreciable portions of the ESDA distributions being negative in both Sub A and Sub B. The mean Bz ESDA values were the lowest in Sub B and the highest in the monomer. The distribution pattern of Tyr55 was quite different between Sub A and Sub B. In Sub A the distribution peak was highly negative (mean -0.601 eV; see Table 4), while in Sub B it was similar with those of Tyr224 and Tyr314 (mean -236 eV), and with one in the monomer (mean -0.191 eV). The mean ESDA values for Tyr228 were somewhat similar in Sub A and Sub B, but were significantly lower in the monomer.

The solvent reorganization energies (λ_S^{wj}) (Table 4) for Bz and Tyr 228 were highest in Sub B (slightly more than in Sub A at 1.16- and 1.03-fold, respectively) but much lower in the monomer at 1.18- to 1.37-fold and 1.2- to 1.4-fold, respectively), whilst that for Tyr314 was essentially equally high in all three forms (Sub A, Sub B and the monomer).

Polarity around Iso

The polarity around Iso may be related to number of water molecules near it. The radial distribution functions of water molecules (G(r)) near the heteroatoms of Iso, which is considered to represent water molecules steadily located near the heteroatoms of Iso, is shown in Fig. S8 (Supporting Information). The G(r) functions of Sub A and Sub B in the DAOB dimer are shown in red and blue respectively, whilst that for the

monomer is shown in black and is taken from previous work[35] for comparison. In Sub B an average of 1.1 water molecules were located near O2 and N3 (see Chart 1 for atom notations), one molecule near O4, and approximately two molecules were located near N5. However, in Sub A no water molecule existed near these heteroatoms in Iso as in the monomer.

These results, and the G(r) functions in Fig. S8 (Supprting Information), suggest that the polarity near Iso was higher in Sub B than in Sub A. This is in accordance with the results of the dielectric constants ε_0^{DA} and ε_0^{DB} (2.53 and 2.64 respectively, Table 3) in the DAOB dimer, which suggests polarity near Iso, Bz, Tyr55 and Tyr228 in Sub A is a little lower than that near Iso, Bz and Tyr228 in Sub B (see descriptions on ε_0^{DA} and ε_0^{DB} below eqn (2)). In the monomer the value of ε_0^{DA} near Iso, Bz, Tyr224 and Tyr228 was 2.45 (Table S2, Supporting Information) and no water molecule was also found near heteroatoms of Iso. It should be noted that molecules other than water may also influence the polarity, such as any ionic groups near Iso.

Fig. S9 (Supporting Information) shows water molecules existing 0.7 nm from IsoN5. In Sub A Iso, Bz, Tyr55 and Tyr228 are shown, and in Sub B Iso, Bz and Tyr228 in a snapshot. The static dielectric constant in these domains are ε_0^{DA} for Sub A and ε_0^{DB} for Sub B. In Sub A there exist three water molecules, but no water molecule near Iso within 0.5 nm, as predicted by G(r) function in Fig. S8. In Sub B some water molecules exist near Iso within 0.5 nm. These results are in accordance with the interpretation about the polarity near Iso described above.

Emission peak of fluorescence spectrum of a flavoprotein may be related to the static dielectric constant near Iso (ε_0^{DA} for Sub A and ε_0^{DB} for Sub B). Fluorescence spectrum

of DAOB dimer is shown in Fig. S1 (Supporting Information). The emission peak was 524 nm, while the peak of holoDAAO dimer is around 530 nm.[52] The static dielectric constants near Iso were 2.4 – 2.7 in DAOB dimer and monomer, while it is 5.8 - 5.9 in holoDAAO dimer and monomer.[33,36] These results are in accordance with those of the static dielectric constant near Iso obtained by the present ET analyses. Similar result with respect to the relationship between the static dielectric constant near the donor and Iso, and emission peak of Iso was obtained in flavodoxins.[32] However, it should be noted that the fluorescence spectrum of Iso depends on two factors, polarity around Iso, (Stokes Shift) and hydrogen bond (H-bond) structure between Iso* and nearby amino acids. Iso contains five hydrogen bonding acceptors and one donor (see Chart 1). The energy shift of Iso upon H-bond formations has been studied by a MO method for the ground state of Iso.[54] It is well known that H-bond or proton transfer phenomena are different between the ground and excited states in general. Accordingly, the modifications of the transition energies of Iso by H-bond formations should be examined for Iso* by MO method.

Difference in the charge densities Iso and Iso* between Sub A and Sub B with and without H-bonds.

Charge densities of atoms in free Iso and Iso with H-bond cluster were shown in Table S3 (Supporting Information). Numbering of atoms in Iso and H-bonded amino acids are shown in Fig. S11 (Supporting Information). The charge densities were not much different between Sub A and Sub B. The charge densities with the differences greater than 0.01 are indicated in green in Table S3. In the ground state of Iso the atom O7 (O4 in the Chart 1), H19 and H21 displayed the differences greater than 0.01 between Sub A and Sub B. In the excited state many more atoms displayed the greater differences.

Atom N1 (N1 in Chart 1) displayed quite large difference by 0.03 between Sub A and Sub B. The differences were 0.25 in C8 (C4a in Chart 1), 0.24 in C11 (C6 in Chart 1), 0.28 in H29 (H connected to N10 in Chart 1), and 0.34 in H31 (H connected to N10 in Chart 1). H-bond cluster considerably modified the charge densities of Iso in the excited state, for example, by 0.027 in C10 (C5a in Chart 1) of Sub A, by 0.041 in C11 (C6 in Chart 1) of Sub A and by 0.017 in C11 of Sub B, by 0.05 in N27 (N10 in Chart 1) of Sub A. These differences in the charge densities between Sub A and Sub B in the excited state may be related to the difference in the ET rates between Sub A and Sub B. Fig. S12 shows molecular orbitals of HOMO and LUMO of Iso in the ground and excited states without H-bond clusters. The LUMO and HOMO displayed considerable difference between the ground and excited states.

Relationship between logarithmic ET rate and Rc

The dependence of the logarithmic ET rate on the donor-acceptor distance (edge to edge distance, Re) is called as Dutton ruler.[44] The relationship between logarithmic ET rates and the donor-acceptor distances is shown in the DAOB dimer and the monomer in Fig. 6, where Rc was used as the donor-acceptor distance. The relationship should be examined separately with each kind of ET donor, otherwise linear relations of the logarithmic ET rates with Rc cannot be expected. It has been noted that the Rc rather than the Re is responsible for the relationship between logarithmic ET rate and Rc in flavoproteins[50, 51] in contrast to photosynthetic systems where Re was used as the donor-acceptor distance.[44] In all three DAOB systems excellent linear relations were obtained, including in the monomer. The slopes for Trp were similar in the two dimer subunits (-22.1 and -22.2 in Sub A and Sub B, respectively), and a little higher in the

monomer (-24.7), and likewise for Tyr they were -13.0, -13.2 and -14.6 in Sub A, Sub B and the monomer, respectively. Thus, the slopes for both Trp and Tyr were quite similar between Sub A and Sub B, but a little higher in the monomer than those in the dimer. The relationship between logarithmic ET rate and the donor-acceptor distances was also examined with Re as shown in Figure 7. The ln Rate vs Re relationship also displayed linear functions. The slopes of the approximate functions of Trp were -19.1 in Sub A, -19.8 in Sub B and -19.7 in Monomer, while those of Tyr were -14.2 in Sub A, -14.4 in Sub B, and -15.0 in Monomer. These values were quite different from those with Rc as the donor-acceptor distance, which suggests that Rc and Re are proportional.

The Re values should be dependent on inter-planar angles between Iso and donors. Fig. S10 (Supporting Information) shows the relationship between Iso and main donors, Tyr228 and Bz. In this Figure the logarithmic ET rates did not display any clear relations with the inter-planar angles. This should be ascribed that any theories including KM rate do not explicitly include the angular-dependence between the donor and acceptor as Förster-type energy transfer rate.

Numerical elucidation of differences in the fluorescence lifetimes between two subunits in the DAOB dimer and between the dimer and monomer

The observed fluorescent lifetimes of DAOB were 4.77 ps in Sub A and 0.848 ps in Sub B in the dimer. It is then of interest to elucidate the difference in the lifetimes (ET rates) between the two subunits in the DAOB dimer. The logarithmic ET rate expressed by eqn (1) or eqn (4) may be rewritten as eqns (16)–(19):

$$\ln EC^{w} = \ln\left[\frac{\nu_0^{w}}{1+\exp\left\{\beta^{w}(R_j - R_0^{w})\right\}}\right], \qquad (16)$$

$$\ln SQ^{w} = \ln\left\{\sqrt{\frac{k_B T}{4\pi\lambda_S^{wj}}}\right\}, \quad (17)$$

$$GT^{w} = \Delta G_w^0 - e^2 / \varepsilon_0^p R_j + \lambda_S^{wj} + ES_j(k), \quad (18)$$

$$GTRAM^{w} = -\frac{\left\{GT^{wj}\right\}^2}{4\lambda_S^{wj} k_B T}. \quad (19)$$

The logarithmic ET rate can then be obtained from eqn (20),

$$\ln k_{ET}^{w} = \ln EC^{w} + \ln SQ^{w} + GTRAM^{w}. \quad (20)$$

In these equations, q is Trp, Tyr or Bz, while $\ln k_{ET}^{w}$ is the logarithm of the ET rate given by eqn (1) for Trp and Tyr, and by eqn (4) for Bz. The meanings of each term in these equations are described below eqns (1) and (4), where EC^{w} is the electronic coupling term, and GT^{w} is the total free energy gap and appeared in exponential functions of the rates. These values for several donors are listed in Table 5.

The contributions of the Bz and Tyr228 ET rates to the total rates (inverse of the fluorescence lifetime) were ca. 90% in all the systems. Given that the values of $\ln k_{ET}^{w}$ in Bz were -2.59 in Sub A and -0.114 in Sub B, this raises the question as to why the rate of Bz was some 22.7-fold slower in Sub A than in Sub B. The values of $\ln EC^{w}$ for Bz were slightly higher in Sub A than in Sub B. The values of $\ln SQ^{w}$ were similar between Sub A and Sub M, but the absolute value of $GTRAM^{w}$ for Bz was 2.1-fold higher in Sub A than in Sub B. The $\ln k_{ET}^{w}$ (Table 5) was obtained as sum of these values, according to eqn (20), and these were found to agree well with the $\ln k_{ET}^{w}$ values (Table 5). That the value of $\ln k_{ET}^{w}$ was smaller in Sub A (slower ET rate) than in Sub B was hence ascribed to the two-fold larger absolute value of $GTRAM^{w}$ in Sub A than in

Sub B. $GTRAM^w$ is mainly determined by GT^w eqn (16), because there was very little variation in SQ between the subunits. The values of ΔG_w^0 (given by eqn (6)) were similar in the two subunits, whilst the ESDA ($-e^2 / \varepsilon_0^p R_j$), solvent reorganization energy (λ_S^{wj} from eqn (5)) and ES_{Bz} (from eqn (12)) were all quite similar (1.01- to 1.16-fold difference) in the two subunits (Table 4). The values of GT^w for Bz, obtained by the sum of each term according to eqn (18), were 1.32 fold higher in Sub A than in Sub. This is the reason why the absolute value of $GTRAM^w$ from eqn (19) was larger in Sub A than in Sub B, and so that the lifetime of Sub A is much longer than Sub B (ET rate of Sub A is much slower than Sub B, and note that $GTRAM^w$ is always negative, see eqns (19) and (20)). The reason why the absolute value of GT^w was greater in Sub A than in Sub B is due to the smaller value of λ_S^{wj} in Sub A than in Sub B, which in turn was due to the shorter Rc in Sub A than in Sub B and to the smaller dielectric constant of ε_0^{DA} than of ε_0^{DB}, as revealed by eqn (5).

It is also of interest why the fluorescent lifetime of the monomer is much longer than in the DAOB dimer, that is 12.6- and 70.8-fold longer than that for Sub A and Sub B, respectively.[34] The ET rate from Bz was the fastest among the donors in the monomer. The values of $\ln EC^w$ and $GTRAM^w$ for Bz in the monomer were 1.1- and 2.3-fold lower than in Sub A and 1.02- and 4.64-fold lower than in Sub B, respectively, although $\ln SQ^w$ was only 1.03- and 1.05-fold higher than in Sub A and Sub B, respectively. Thus, the $GTRAM^w$ in the monomer was markedly smaller than those in Sub A and Sub B and this is likely to be the principal reason why the value of $\ln k_{ET}^w$ in the monomer was much smaller, and so the fluorescence lifetime was much longer, than

those in the dimer subunits. $GTRAM^w$ is mainly dependent on GT^w (eqn (19)), which is itself derived from the summation of the ΔG_w^0, ESDA, λ_S^{wj} and ES_{Bz} values (eqn (18)). The values of ΔG_w^0, ESDA and λ_S^{wj} in Bz were not dramatically different (1.1- to 1.55-fold difference) between the monomer and the dimer subunits (Table 5). However, the NetES energy (ES_{Bz}) was markedly higher in the monomer than in the dimer subunits. Thus, the main reason why the fluorescent lifetime is much longer (slower ET rate) in the monomer than those in the dimer is due to greater NetES energy (ES_{Bz}) in the monomer compared to in the dimer. This was ascribed to the inter-subunit interactions in terms of the Rc and dielectric constant, as stated above.

The ET rate from Tyr228 to Iso* was 2.4-fold slower in Sub A than in Sub B, but some 660-fold faster than that in the monomer. That the ET rates from Tyr228 were much faster in the dimer subunits than in the monomer, despite that the donor-acceptor Rc distances of the dimer were ~1.2-fold longer than that in the monomer, is because the absolute values of $GTRAM^w$ in the dimer were much smaller than that in the monomer. The greater absolute $GTRAM^w$ value in the monomer was mainly ascribed to the low λ_S^{qj} with a shorter Rc and a low ε_0^{DA} (Table S2; Supporting Information).

IV Discussion

During 1980-2000 a number of workers have reported on ET and dark electron transfer in small molecules and in proteins.[55-60] In these works, however, it was difficult to determine theoretically and experimentally individual ET parameters contained in the ET rates. Our approach to analyze ET rate quantitatively is that 1) fluorescence decays or lifetimes of flavoproteins are obtained from experimental results, 2) atomic

coordinates of a flavoprotein are determined by MDS methods, 3) ET rates are evaluated with an analytical theory like KM rate or sometimes Marcus rate, 4) the several unknown ET parameters are determined by a non-linear least squares method according to Marquardt algorithm. By using the above described strategy, we have reported on ET mechanisms on several flavoproteins.[28-33,35,36]

Experimentally, the DAOB dimer displays two fluorescent species with lifetimes of 0.85 ps and 4.8 ps, which have been identified as being derived from Sub B and Sub A, respectively. The structural basis for the heterogeneity has been studied by means of MDS and ET analysis. The contributions of the ET rates from Bz and Tyr228 to the total rates were ~90% in all systems, including in the monomer. The Rc distances of the main donors in Sub A and Sub B respectively, were 0.66 and 0.68 for Bz, compared to 0.96 and 0.99nm for Tyr228, which did not correlate with the differences in the ET rates. This is in contrast to that for the DAAO holodimer,[36] where the difference in the fluorescence lifetime between the monomer and dimer was attributed to the difference in Rc. The ET rates of Bz were significantly different between Sub A and Sub B, being the second fastest in Sub A and the fastest in Sub B.

Decomposing the ET rate into the electronic coupling (EC^w), square root (SQ^w) and exponential ($GTRAM^w$) terms revealed that the main reason for the faster ET rate of Bz in Sub B was the two-fold larger absolute $GTRAM^w$ value in Sub A than in Sub B. This in turn was ascribed to the greater λ_S^{wj} in Sub B than in Sub A, because the Rc was longer and the dielectric constant was smaller in Sub B than in Sub A. That the fluorescence lifetime was 12.6- and 70.8-fold shorter (much faster ET rate) in the dimer than in the monomer was explained by the 2.3- and 4.64-fold larger $GTRAM^w$ values in

the dimer compared to the monomer, which in turn was due to the much higher NetES energy (ES_{Bz}) in the monomer compared to the dimer.

Original Marcus theory[42,43] was derived assuming that the donor and acceptor are spherical (also KM rate). It is not unreasonable to use Rc as the donor-acceptor distance for the ET analyses. If the molecules are spherical, Rc and Re should be identical. Firstly the relationship between logarithmic ET rate and the donor-acceptor distances has been experimentally obtained with Re in photosynthetic systems.[44] In these systems ET rates were slower (longer than 0.63 ps in the lifetimes), and so the distances were longer, comparing to in flavoproteins. When the distance is quite long, and so the ET rate is relatively slow, the effects of the difference between Rc and Re on the theoretical ET rates or the logarithmic rates vs the donor-acceptor distance relationship may not be significant. When the donor-acceptor distances become shorter, and so ET rates are faster than ca. 0.5 ps in lifetimes, the behavior of logarithmic ET rates vs the donor-acceptor distances are quite different. The logarithmic ET rates deviates from a linear function of Rc which was obtained at relatively longer distances.[50,51]

The relationship between logarithmic ET rate and Rc in DAOB was analyzed with the EC^w, SQ^w and $GTRAM^w$ terms. If it can be explained by the EC^w term alone (or principally) then the slopes should equate to or be close to - β^w (*w*; Trp, Tyr and Bz; see Table 2). However, there were considerable discrepancies between the slope of ln Rate vs Rc function and - β^w in Tyr. The logarithmic ET rate could be decomposed into its constitutive three terms (eqn (20)), where the dependence of the logarithmic ET rate on Rc could be expressed as a sum of those for EC^w and $GTRAM^w$, since the variation

in $\ln SQ^{w}$ between Sub A, Sub B and the monomer was essentially negligible compared to the two other terms. Fig. 8 shows relationship between $GTRAM^{w}$ and Rc in Tyr. The slopes were -6.98 in Sub A, -7.31 in Sub B and -8.44 in Monomer. Sums of these slopes and $-\beta^{Tyr}$ were -13.2 in Sub A, -13.6 in Sub B and -14.7 in Monomer, which are compared to the slopes in Fig. 6, -13.0 in Sub A, -13.2 in Sub B and -14.6 in Monomer. The slope calculated based on logarithmic ET rate vs Rc function was practically identical to the sum of the slope in Fig. 8 and $-\beta^{Tyr}$ in each system. This implies that the slope in the $GTRAM^{w}$ vs Rc relationship considerably contributes to the slope in the relationship between logarithmic ET rate and Rc. Further it is concluded that a linear relationship between the logarithmic ET rates and Rc is obtained only when $GTRAM^{w}$ linearly depends on Rc.

It has been reported that the relationship between logarithmic ET rate and Rc in flavin mononucleotide (FMN) binding proteins displays a bell-shaped (not linear) function in the ET processes from Trp to Iso* when the ET rates are ultrafast (10–15 ps^{-1}).[52] This work emphasized that the $GTRAM^{w}$ term plays the main role determining the bell-shaped behaviour. However, a bell-shape was not observed in the ET from Tyr to Iso* in the flavodoxin from *Helocobactor pylori*,[32] even though the ET rate was ultrafast at 6–23 ps^{-1}. Thus, the bell-shape behaviour can only be observed when GT^{w} linearly depends on Rc, and so $GTRAM^{w}$ becomes a parabolic function of Rc. In DAOB, the rates (0.01–0.9 ps^{-1}) were much slower than those in the FMN binding proteins and the flavodoxins, and in addition the $GTRAM^{w}$ was a linear function of Rc, not parabolic.

V Conclusion

Experimental fluorescence dynamics of DAOB dimer displays two lifetime components, 0.85 ps and 4.8 ps. It was identified that the fluorescence with the shorter lifetime is from Sub B and one with the longer lifetime from Sub A. The difference in the lifetimes was mainly ascribed to differences in the ET rates from Bz to Iso*in the two subunits. This is because the absolute value of GT^w for ET from Bz in Sub A is greater than that in Sub B.

Relationship between logarithmic ET rate and Rc displayed linear functions both for Tyrs and for Trps as ET donors. Sum of the slopes of the $GTRAM^w$ vs Rc functions and of ln EC^w vs Rc functions were almost identical with the slopes of $\ln k_{ET}^w$ vs Rc functions, which reveals that the $GTRAM^w$ term considerably contributes to the slope of the $\ln k_{ET}^w$ vs Rc function.

Acknowledgements

This work was financially supported by The Chulalongkorn University Dutsidi Phiphat Scholarship. Thanks are also given to The National e-Science Infrastructure Consortium Project for computing facilities.

References

1 R. Miura, C. Setoyama, Y. Nishina, K. Shiga, I. Miyahara, H. Mizutani and K. Hirotsu, *J. Mol. Catal. B: Enzymatic*, 2001, **12**, 43-52.

2 V. I. Tishkov and S. V. Khoronenkova, *Biochemistry (Moscow)*, 2005, **70**, 40-54.

3 L. Pollegioni, L. Piubelli, S. Sacchi, M. S. Pilone and G. Molla, *Cell. Mol. Life Sci.*, 2007, **64**, 1373-1394.

4 T. Kawazoe, H. K. Park, S. Iwana, H. Tsuge and K. Fukui, *Chem. Rec.*, 2007, **7**, 305-315.

5 S. Sacchi, L. Caldinelli, P. Cappelletti, L. Pollegioni and G. Molla, *Amino Acids*, 2012, **43**, 1833-1850.

6 C. Madeira, M. E. Freitas, C. Vargas-Lopes, H. Wolosker and R. Panizzutti, *Schizophr. Res.*, 2008, **101**, 76-83.

7 M. P. M. Boks, T. Rietkerk, M. H. van de Beek, I. E. Sommer, T. J. de Koning and R. S. Kahn, *Eur. Neuropsychopharmacol.*, 2007, **17**, 567-572.

8 M. Katane, N. Osaka, S. Matsuda, K. Maeda, T. Kawata, Y. Saitoh, M. Sekine, T. Furuchi, I. Doi, S. Hirono and H. Homma, *J. Med. Chem.*, 2013, **56**, 1894-1907.

9 M. L. Fonda and B. M. Anderson, *J. Biol. Chem.*, 1968, **243**, 5635-5643.

10 S. W. Henn and G. K. Ackers, *Biochemistry*, 1969, **8**, 3829-3838.

11 S. W. Henn and G. K. Ackers, *J. Biol. Chem.*, 1969, **244**, 465-470.

12 K. Yagi and N. Ohishi, *J. Biochem. (Tokyo)*, 1972, **71**, 993-998.

13 E. Antonini, M. Brunori, M. R. Bruzzesi, E. Chiancone and V. Massey, *J. Biol. Chem.*, 1966, **241**, 2358-2366.

14 H. Tojo, K. Horiike, K. Shiga, Y. Nishina, H. Watari and T. Yamano, *J. Biol. Chem.*, 1985, **260**, 12607-12614.

15 H. Tojo, K. Horiike, K. Shiga, Y. Nishina, H. Watari and T. Yamano, *J. Biol. Chem.*, 1985, **260**, 12615-12621.

16 H. Mizutani, I. Miyahara, K. Hirotsu, Y. Nishina, K. Shiga, C. Setoyama and R. Miura, *J. Biochem.*, 1996, **120**, 14-17.

17 A. Mattevi, M. A. Vanoni, F. Todone, M. Rizzi, A. Teplyakov, A. Coda, M. Bolognesi and B. Curti, *Proc. Natl. Acad. Sci. USA*, 1996, **93**, 7496-7501.

18 A. Karen, N. Ikeda, N. Mataga and F. Tanaka, *Photochem. Photobiol.*, 1983, **37**, 495-502.

19 A. Karen, M. T. Sawada, F. Tanaka and N. Mataga, *Photochem. Photobiol.*, 1987, **45**, 49-53.

20 D. Zhong and A. H. Zewail, *Proc. Natl. Acad. Sci. USA*, 2001, **98**, 11867-11872.

21 P A van den Berg, A van Hoek, C D Walentas, R N Perham, and A J Visser, *Biophys J.* 1998, **74**, 2046–2058.

22 P. A. van der Berg and A. J. W. G. Visser, *New Trends in Fluorescence Spectroscopy. Applications to Chemical and Life Sciences*, Springer, Berlin, 2001.

23 N. Mataga, H. Chosrowjan, Y. Shibata, F. Tanaka, Y. Nishina and K. Shiga, *J. Phys. Chem. B*, 2000, **104**, 10667-10677.

24 N. Mataga, H. Chosrowjan, S. Taniguchi, F. Tanaka, N. Kido and M. Kitamura, *J. Phys. Chem. B*, 2002, **106**, 8917-8920.

25 H. Chosrowjan, S. Taniguchi, N. Mataga, F. Tanaka, D. Todoroki and M. Kitamura, *J. Phys. Chem. B*, 2007, **111**, 8695-8697.

26 H. Chosrowjan, S. Taniguchi, N. Mataga, F. Tanaka, D. Todoroki and M. Kitamura, *Chem. Phys. Lett.*, 2008, **462**, 121-124.

27 H. Chosrowjan, S. Taniguchi, N. Mataga, T. Nakanishi, Y. Haruyama, S. Sato, M. Kitamura and F. Tanaka, *J. Phys. Chem. B*, 2010, **114**, 6175-6182.

28 N. Nunthaboot, F. Tanaka, S. Kokpol, H. Chosrowjan, S. Taniguchi and N. Mataga, *J. Phys. Chem. B*, 2008, **112**, 13121-13127.

29 N. Nunthaboot, S. Pianwanit, S. Kokpol and F. Tanaka, *Phys. Chem. Chem. Phys.*, 2011, **13**, 6085-6097.

30 K. Lugsanangarm, S. Pianwanit, S. Kokpol, F. Tanaka, H. Chosrowjan, S. Taniguchi and N. Mataga, *J. Photochem. Photobiol. A*, 2011, **219**, 32-41.

31 N. Nunthaboot, N. Kido, F. Tanaka, K. Lugsanangarm, A. Nueangaudom, S. Pianwanit and S. Kokpol, *J. Photochem. Photobiol. A*, 2013, **252**, 14-24.

32 K. Lugsanangarm, S. Pianwanit, A. Nueangaudom, S. Kokpol, F. Tanaka, N. Nunthaboot, K. Ogino, R. Takagi, T. Nakanishi, M. Kitamura, S. Taniguchi and H. Chosrowjan, *J. Photochem. Photobiol. A*, 2013, **268**, 58-66.

33 A. Nueangaudom, K. Lugsanangarm, S. Pianwanit, S. Kokpol, N. Nunthaboot and F. Tanaka, *Phys. Chem. Chem. Phys.*, 2012, **14**, 2567-2578.

34 K. Yagi, F. Tanaka, N. Nakashima and K. Yoshihara, *J. Biol. Chem.*, 1983, **258**, 3799-3802.

35 A. Nueangaudom, K. Lugsanangarm, S. Pianwanit, S. Kokpol, N. Nunthaboot and F. Tanaka, *J. Photochem. Photobiol. A*, 2012, **250**, 6-17.

36 A. Nueangaudom, K. Lugsanangarm, S. Pianwanit, S. Kokpol, N. Nunthaboot and F. Tanaka, *Phys. Chem. Chem. Phys.*, 2014, **16**, 1930-1944.

37 D. A. Case, T. A. Darden, I. T.E. Cheatham, C. L. Simmerling, J. Wang, R. E. Duke, R. Luo, M. Crowley, R. C. Walker, W. Zhang, K. M. Merz, B. Wang, S. Hayik, A. Roitberg, G. Seabra, I. Kolossváry, K. F. Wong, F. Paesani, J. Vanicek, X. Wu, S. R. Brozell, T. Steinbrecher, H. Gohlke, L. Yang, C. Tan, J. Mongan, V. Hornak, G. Cui, D. H. Mathews, M. G. Seetin, C. Sagui, V. Babin and P. A. Kollman, 2008, vol. AMBER 10, University of California, San Francisco.

38 J. Wang, P. Cieplak and P. A. Kollman, *J. Comput. Chem.*, 2000, **21**, 1049-1074.

39 C. I. Bayly, P. Cieplak, W. Cornell and P. A. Kollman, *J. Phys. Chem.*, 1993, **97**, 10269-10280.

40 U. Essmann, L. Perera, M. L. Berkowitz, T. Darden, H. Lee and L. G. Pedersen, *J. Chem. Phys.*, 1995, **103**, 8577-8593.

41 J.-P. Ryckaert, G. Ciccotti and H. J. C. Berendsen, *J. Comput. Phys.*, 1977, **23**, 327-341.

42 R. A. Marcus, *J. Chem. Phys.*, 1956, **24**, 966-978.

43 R. A. Marcus, *Annu. Rev. Phys. Chem.*, 1964, **15**, 155-196.

44 C. C. Moser, J. M. Keske, K. Warncke, R. S. Farid and P. L. Dutton, *Nature*, 1992, **355**, 796-802.

45 T. Kakitani and N. Mataga, *J. Phys. Chem.*, 1985, **89**, 8-10.

46 A. Yoshimori, T. Kakitani, Y. Enomoto and N. Mataga, *J. Phys. Chem.*, 1989, **93**, 8316-8323.

47 N. Matsuda, T. Kakitani, T. Denda and N. Mataga, *Chem. Phys.*, 1995, **190**, 83-95.

48. H. B. Gray, J. R. Winkler, *Pure & Appl. Chem.*, 1992, **64**, 1257-1262.

49 V. Vorsa, T. Kono, K.F. Willey, N. Winograd, *J. Phys. Chem. B* 1999, **103**, 7889 - 7895.

50 F. Tanaka, H. Chosrowjan, S. Taniguchi, N. Mataga, K. Sato, Y. Nishina and K. Shiga, *J. Phys. Chem. B*, 2007, **111**, 5694-5699.

51 F. Tanaka, R. Rujkorakarn, H. Chosrowjan, S. Taniguchi and N. Mataga, *Chem. Phys.*, 2008, **348**, 237-241.

52 N. Nunthaboot, K. Lugsanangarm, S. Pianwanit, S. Kokpol, F. Tanaka, S. Taniguchi, H. Chosrowjan, T. Nakanishi and M. Kitamura, *Comp. Theor. Chem.*, 2014, **1030**, 9-16.

53 V. Massey, B. Culti, H. Ganther, *J. Biol. Chem.,* 1966, **241**, 2347-2357.

54 K. Nishimoto, Y. Watanabe, K. Yagi, *Biochim. Biophys. Acta*, 1978, **526**, 34-41.

55 D. N. Beratan, J. N. Betts, J. N. Ounchic, *Science*, 1991, **252**, 1285-1288.

56 D. S. Bendall, *Protein Electron Transfer*. BIOS Scientific Publishers Ltd., Oxford, UK, (1996).

57 H. B. Gray, J. R. Winkler, *Annu. Rev. Biochem.*, 1996, **65**, 537-561.

58 Biophysics of Electron Transfer and Molecular Bioelectronics (Electronics and Biotechnology Advanced (Elba) Forum Series), Nicolini, C., Editor, Springer; (1999)

59 M. Bixon, J. Jortner, Electron transfer—from isolated molecules to biomolecules, in: Advances in Chemical Physics: Electron Transfer – from Isolated Molecules to Biomolecules. Part 1, John Wiley & Sons Inc, Hoboken, NJ, USA, 1999.

60 A. Warshel, W. W. Parson, *Quart. Rev. Biophys*. 2001, **34,** 563–679.

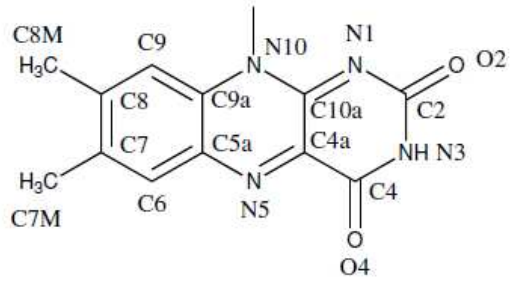

Chart 1 Isoalloxazine ring (Iso) showing the atom notations

Figure captions

Fig. 1	Comparison of the protein structures between Sub A and Sub B in DAOB dimer The structures were shown in yellow for Sub A and in cyan for Sub B in the crystal structures, and in green for Sub A and in magenta for Sub B in the MD snapshots. The crystal structure was taken from Mizutani et al.[16] The MDS calculation was performed at 20 °C. All figures superimposed using Discovery Studio program, alignment by 100% steric and align to consensus of protein.
Fig. 2	Distribution of the Rc values in the DAOB dimer subunits. The distributions of Rc in Bz and five aromatic amino acids with the shortest Rc distances are shown for (A) Sub A and (B) Sub B. The distributions were obtained from 5000 MDS snapshots with 1 ps time intervals.
Fig. 3	Distribution of the logarithmic ET rates in the DAOB subunits for the six fastest ET donors. The observed fluorescence lifetime τ_{obs}^{1} (0.848 ps) was from Sub B and τ_{obs}^{2} (4.77 ps) from Sub A.
Fig. 4	Distribution of the NetES energy in the DAOB subunits for the six fastest ET donors, with that in the monomer for comparison. NetES energies are given by eqn (9) for Tyr and Trp, and by eqn (12) for Bz. Upper, middle and lower panels show the NetES energy of the DAOB Sub A, Sub B and the monomer, respectively.
Fig. 5	Distribution of the ESDA between the photo-products in the DAOB

	subunits, with that in the monomer for comparison. The ESDA, the electrostatic energy (eV) between the photo-products, is expressed as $-e^2/\varepsilon_0^p R_j$ in eqn (1), using the static dielectric constants ε_{DA}^A for Sub A and ε_{DA}^B for Sub B. The acceptor was the Iso anion, and the donors were Trp cations or Tyr cations for aromatic amino acid donors. For Bz, the ESDA was obtained from eqn (11).
Fig. 6	Relationship between logarithmic ET rates and Rc for the Trp and Tyr residues in the DAOB dimer and the DAOB monomer for comparison. Inserts show approximate linear functions of y ($\ln k_{ET}^j$) with x (Rc). The ET rates are expressed in unit of ps^{-1}.
Fig. 7	Relationship between logarithmic ET rates and Re in DAOB. The logarithmic ET rates are taken from Fig. 6. Re represents edge to edge distance.
Fig. 8	Relationship between $GTRAM^w$ and Rc of Tyr in Sub A and Sub B in the DAOB dimer and the DAOB monomer. $GTRAM^w$ is defined by eqn (19). Inserts show approximate linear functions of Y ($GTRAM^w$) with X (Rc).

(A) Superimposition of Sub A with Sub B in the crystal structure

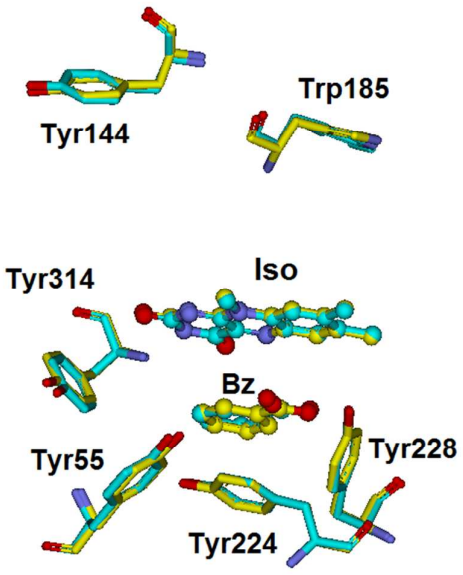

(B) Superimposition of Sub A with Sub B in MDS snapshot

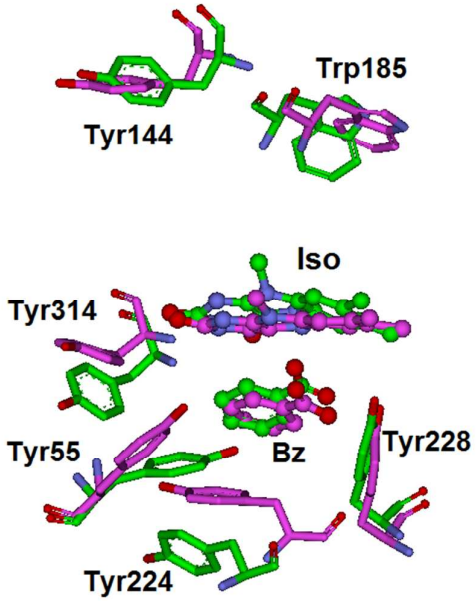

(C) Superimposition of Sub A of crystal structure with Sub A of MDS snapshot

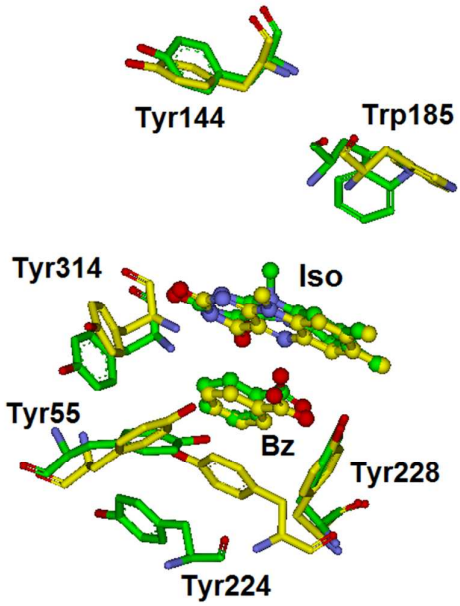

(D) Superimposition of Sub B of crystal structure and Sub B of MDS snapshot

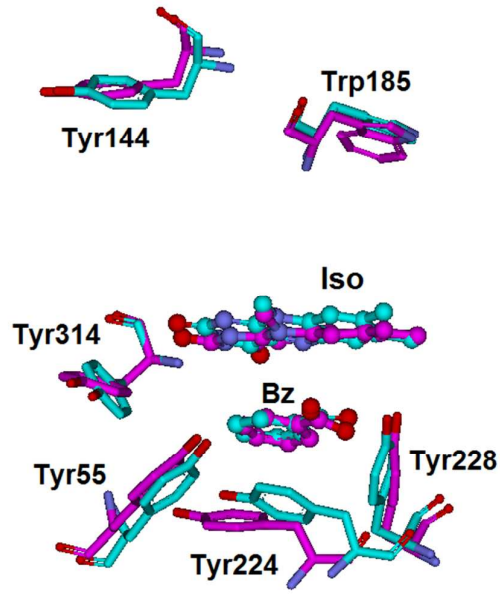

(E) Superimposition of the entire crystal structure and MDS snapshot in DAOB dimer

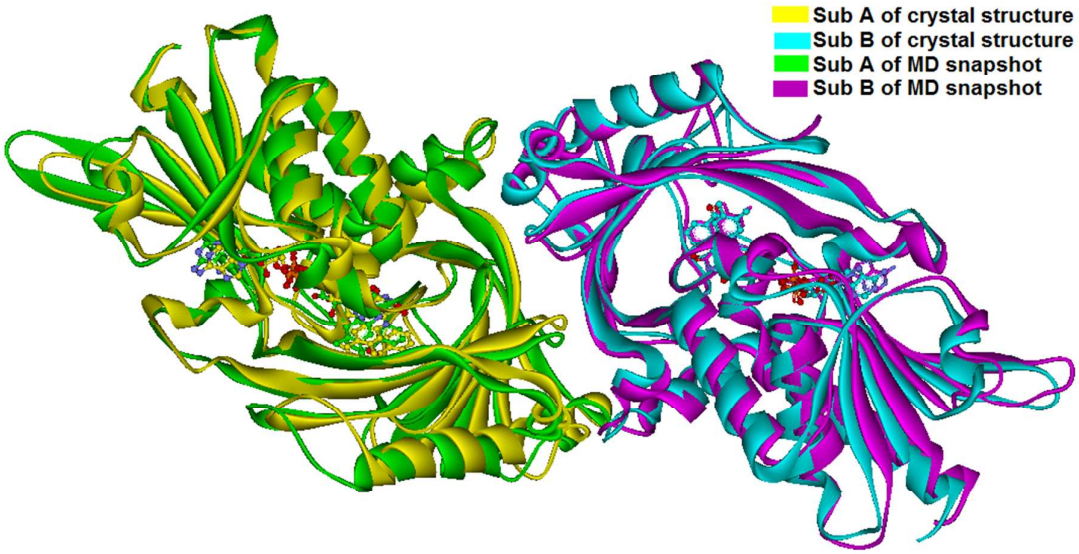

Fig. 1

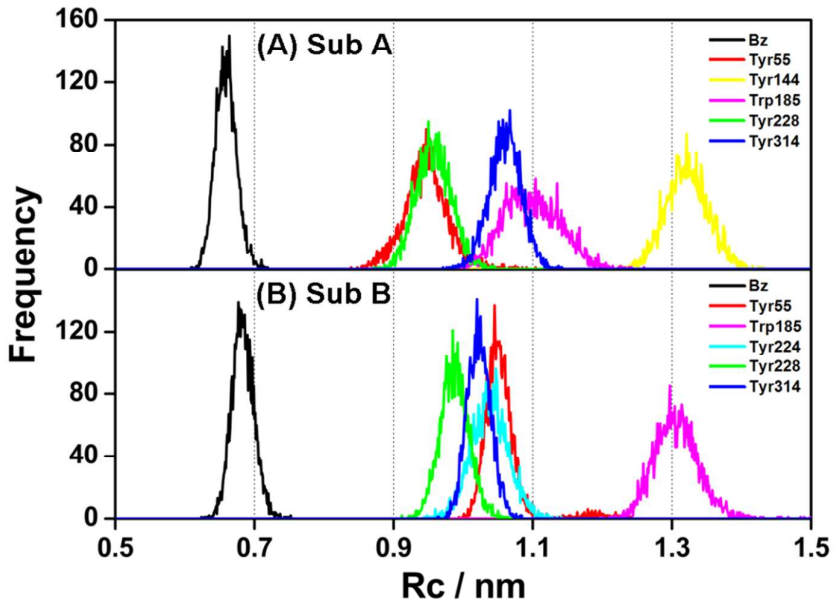

Fig. 2

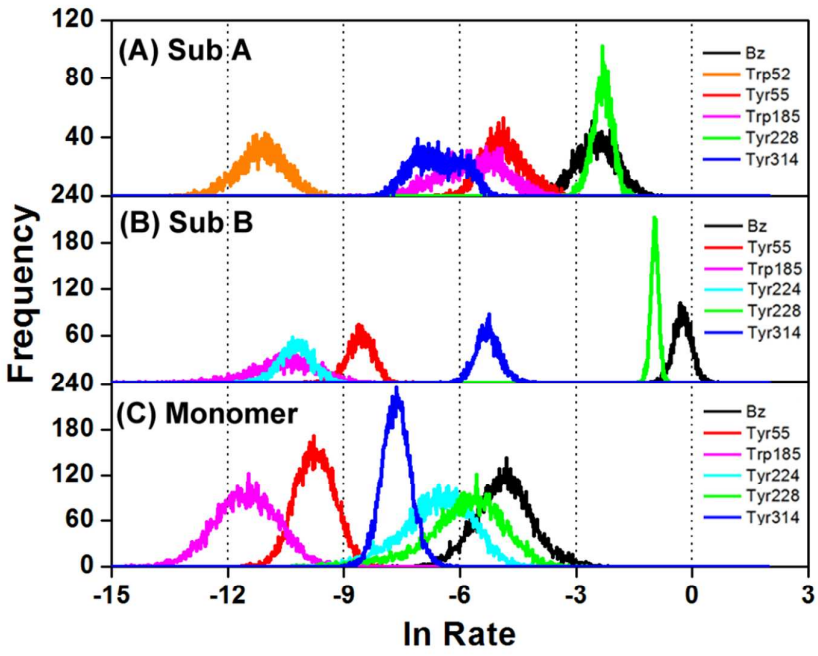

Fig. 3

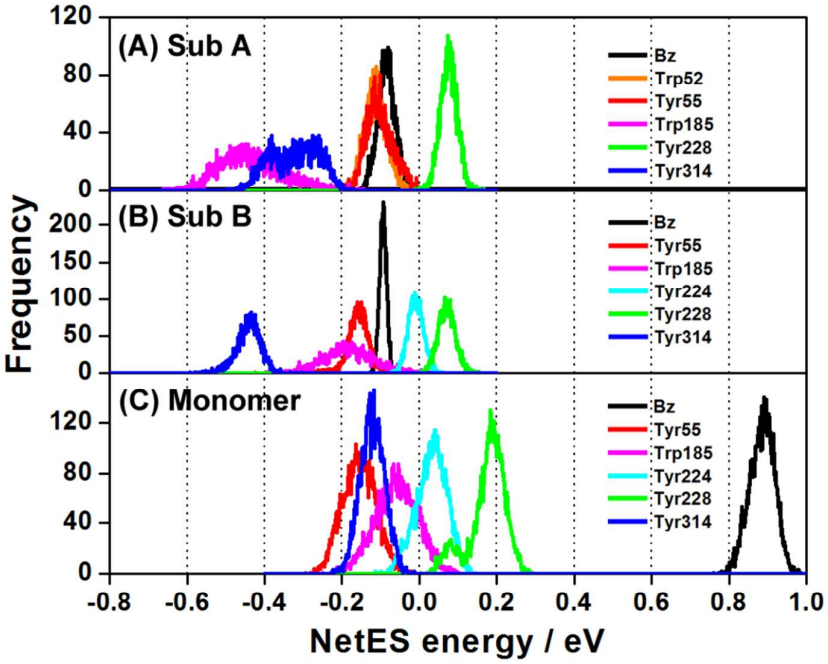

Fig. 4

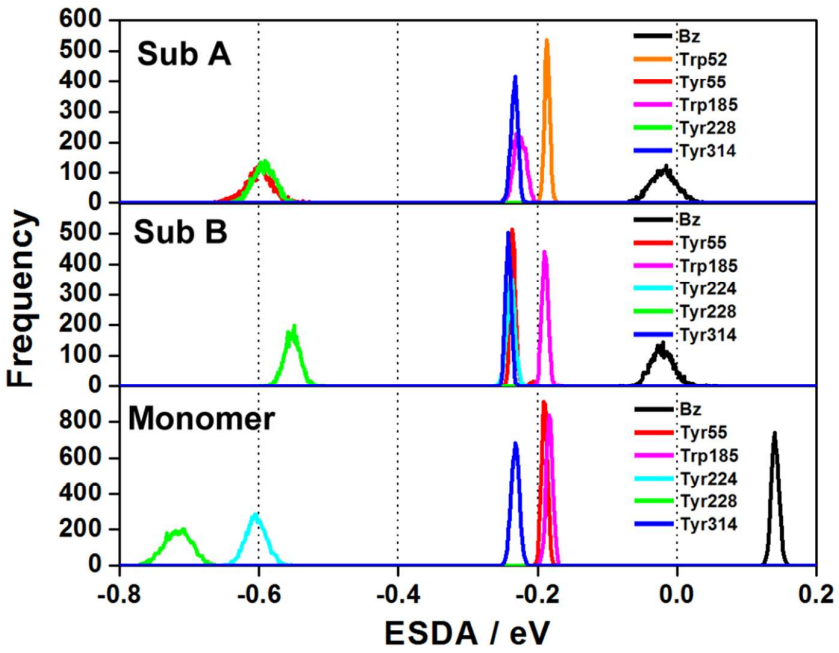

Fig. 5

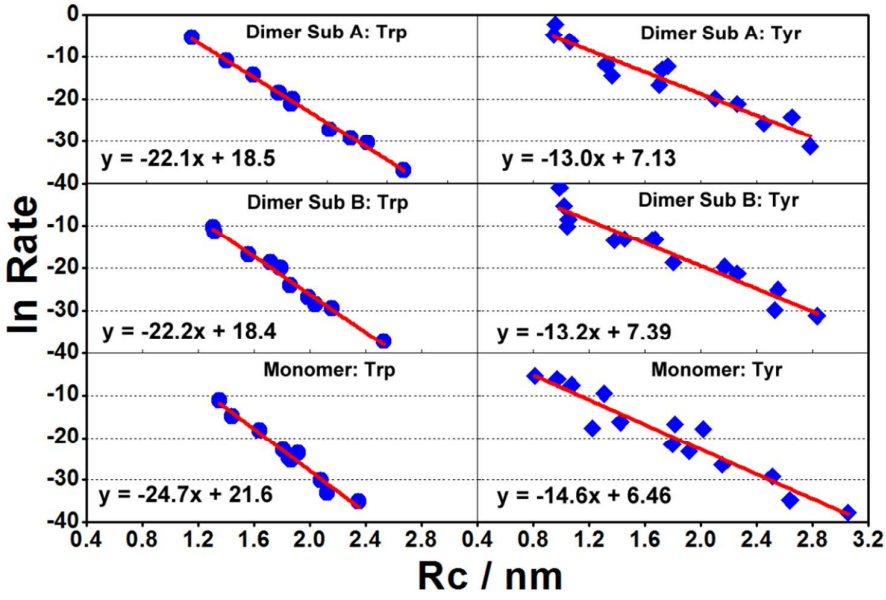

Fig. 6

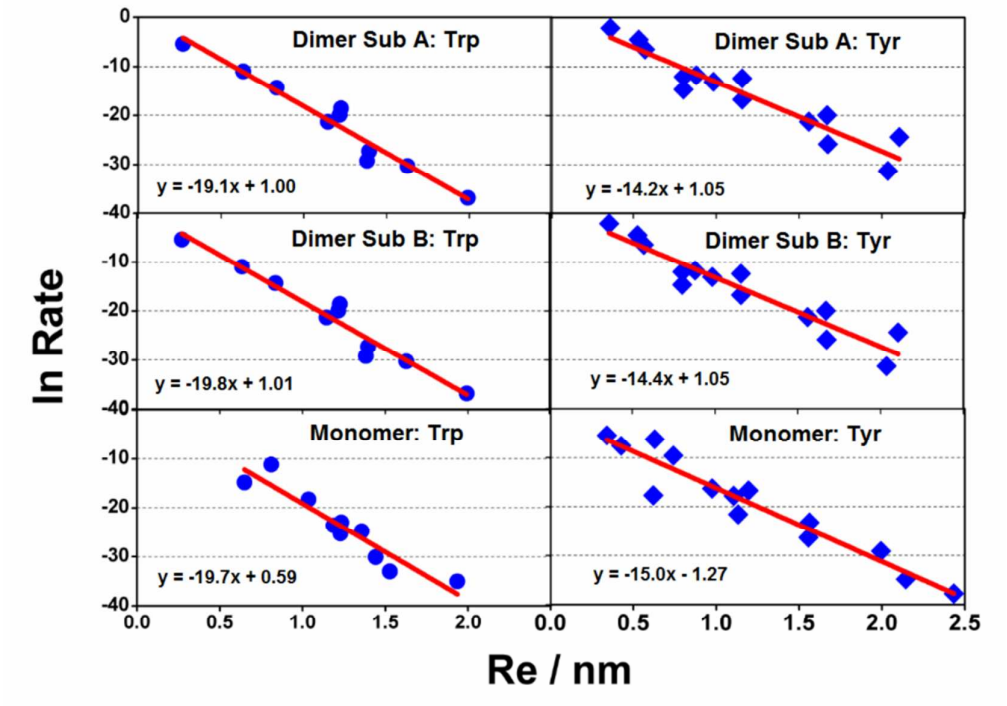

Fig. 7

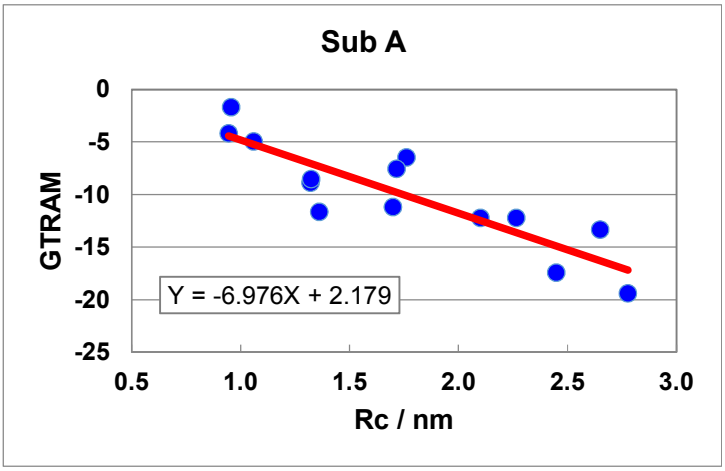

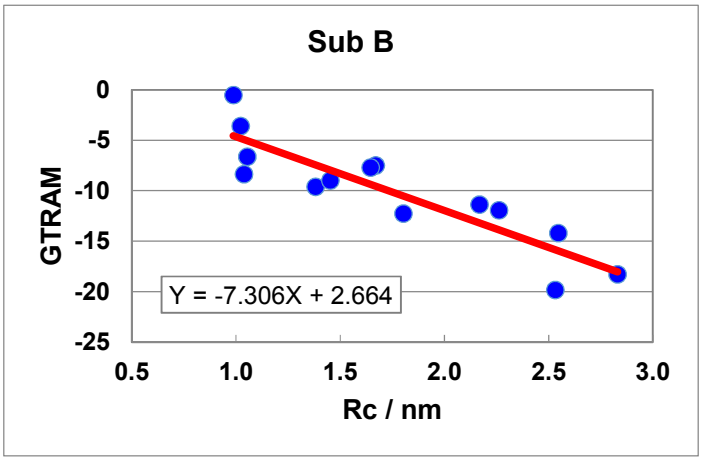

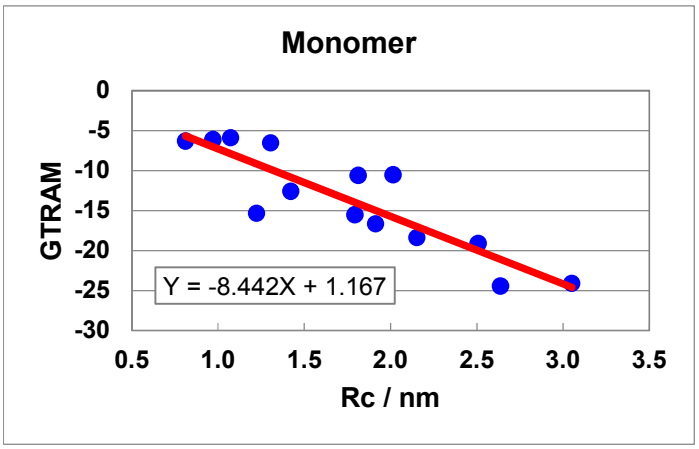

Fig. 8

Table 1 Mean donor-acceptor Rc value in the DAOB subunits and monomer.[a]

Donor	Sub A	Sub B	Monomer
Bz	0.66	0.68	0.61
Tyr55	0.95	1.05	1.31
Tyr144	1.32	1.38	1.43
Trp185	1.10	1.31	1.39
Tyr224	1.32	1.04	0.97
Tyr228	0.96	0.99	0.81
Tyr279	1.36	1.45	1.24
Tyr314	1.06	1.02	1.07

[a] The centre-to-centre distances (Rc) between the Iso acceptor and each donor of Sub A and Sub B in the dimer and in the monomer are shown as the mean values (nm) obtained from 5000 snapshots with 1 ps time intervals. Temperature was 20 °C. Bz denotes benzoate; Sub denotes subunit.

Table 2 ET parameters used for the ET analysis

ν_0^{Trp} [a] (ps^{-1})	ν_0^{Tyr} [a] (ps^{-1})	β^{Trp} [a] (nm^{-1})	β^{Tyr} [a] (nm^{-1})	R_0^{Trp} [a] (nm)	R_0^{Tyr} [a] (nm)	ε_0 [b]	τ_1 [c] (ps)	τ_2 [c] (ps)	ν_0^{Bz} [d] (ps^{-1})	β^{Bz} [d] (nm^{-1})	E_{IP}^{Bz} [d] (eV)
1016	197	21	6.25	0.663	0.499	5.78	0.848	4.77	2001	15.0	7.25

[a] Data taken from Nunthaboot *et al*. (2011).[29]

[b] Data taken from Table S2 (Supporting Information).

[c] Mean shorter (τ_1) and longer (τ_2) lifetimes over ten decays with different emission wavelengths. Data taken from Mataga *et al*. (2000)[23] and listed in Table S1 (Supporting Information).

[d] Data taken from Nueangaudom *et al*. (2012).[35]

Table 3 Best-fit ET parameter[a]

Method[b]	Model[c]		G_{IsoA}^{0} [d] (eV)	G_{IsoB}^{0} [e] (eV)	ε_0^{DA} [f]	ε_0^{DB} [g]	R_0^{Bz} [h] (nm)	χ_A^{2} [i]	χ_B^{2} [j]	χ_T^{2} [k]
1	τ_{obs}^{1} (τ_{calc}^{A})	τ_{obs}^{2} (τ_{calc}^{B})	8.34	8.48	2.65	2.56	0.417	1.79 x 10^{-19}	1.96 x 10^{-30}	8.76 x 10^{-20}
2	τ_{obs}^{1} (τ_{calc}^{B})	τ_{obs}^{2} (τ_{calc}^{A})	8.42	8.43	2.53	2.64	0.462	2.72 x 10^{-21}	2.23 x 10^{-30}	1.36 x 10^{-21}

[a] The five parameters listed here were varied until χ_T^2 became the minimum. Other ET parameters used are listed in Table 2.

[b] Total chi-squared values for Methods 1 and 2 are given by eqns (14) and (15), respectively.

[c] The calculated fluorescence lifetimes for Sub A and Sub B are indicated as τ_{calc}^{A} and τ_{calc}^{B}, respectively. In Method 1 τ_{calc}^{A} was fit with τ_{obs}^{1}, and τ_{calc}^{B} with τ_{obs}^{2}. In Method 2, τ_{calc}^{A} was fit with τ_{obs}^{2} and τ_{calc}^{B} with τ_{obs}^{1}. The calculated lifetimes, τ_{calc}^{A} and τ_{calc}^{B} were 0.848 ps and 4.77 ps, respectively, which completely agreed with those of the observed lifetimes.

[d,e] Standard free energy related to electron affinity of Iso* in [d] Sub A and [e] Sub B.

[f,g] Static dielectric constant around Iso, Bz, Tyr55 and Tyr228 in [f] Sub A, and around Iso, Bz and Tyr228 in [g] Sub B, of which mean Rc values were within 1 nm.

[h] Critical ET distance of Bz as a donor.

[i,j] Chi-squared value for [j] Sub A and [k] Sub B.

[k] Total chi-squared value for Method 1 (χ_1^2) and for Method 2 (χ_2^2).

Table 4 Physical quantities related to the ET in DAOB[a]

Protein	Donor	k_{ET}^{w} (ps^{-1})	$\ln k_{ET}^{w}$ [b]	Rc[c] (nm)	λ_{S}^{wj} [d] (eV)	$ES_j(k)$ [e] (eV)	$ESDA$[f] (eV)
Sub A	Tyr228	1.17×10^{-1}	-2.15	0.957	0.619	0.0750	-0.594
	Bz	7.50×10^{-2}	-2.59	0.659	0.811	-0.0852	-0.0198
	Tyr55	1.14×10^{-2}	-4.48	0.946	0.617	-0.103	-0.601
	Trp185	4.65×10^{-3}	-5.37	1.10	1.83	-0.434	-0.226
	Tyr314	1.58×10^{-3}	-6.45	1.06	1.97	-0.323	-0.234
	Trp52	1.68×10^{-5}	-11.0	1.33	1.90	-0.113	-0.187
Sub B	Bz	8.92×10^{-1}	-0.114	0.683	0.939	-0.0944	-0.0217
	Tyr228	2.80×10^{-1}	-1.27	0.987	0.715	0.0698	-0.553
	Tyr314	6.56×10^{-3}	-5.03	1.02	1.95	-0.442	-0.243
	Tyr55	2.64×10^{-4}	-8.24	1.05	1.97	-0.159	-0.236
	Tyr224	5.38×10^{-5}	-9.83	1.04	1.96	-0.0099	-0.239
	Trp185	3.72×10^{-5}	-10.2	1.31	1.89	-0.183	-0.190
Monomer	Bz	9.92×10^{-3}	-4.61	0.611	0.687	0.898	0.140
	Tyr228	4.23×10^{-3}	-5.46	0.812	0.512	0.172	-0.725
	Tyr224	1.93×10^{-3}	-6.25	0.970	0.538	0.0221	-0.607
	Tyr314	5.05×10^{-4}	-7.59	1.07	1.97	-0.130	-0.232
	Tyr55	6.59×10^{-5}	-9.63	1.31	2.05	-0.171	-0.191
	Trp185	1.37×10^{-5}	-11.2	1.36	1.90	-0.0953	-0.184

[a] Mean values over 5000 snapshots are listed for the DAOB dimer obtained with the ET parameters listed in Table 4, whilst for the monomer the ET parameters listed in Table S2 (Supporting Information) were used.

[b] Logarithmic ET rate of eqn (1).

[c] Centre-to-centre distance (Rc) between Iso and the ET donors.

[d] Solvent reorganization energy, derived from eqn (2).

[e] NetES energies for Tyr and Trp derived from eqn (9), and for Bz from eqn (12).

[f] ES energy between Iso anion and an aromatic amino acid cation or Bz neutral radical.

Table 5 Individual terms of the ET rates in the DAOB Sub A and Sub B of the dimer, and with those for the monomer[a]

Protein	Donor	ln EC^{w} [b]	ln SQ^{w} [c]	$GTRAM^{w}$ [d]	GT^{w} [e] (eV)	ln Rate[f]
Sub A	Tyr228	2.37	-2.87	-1.67	-0.322	-2.15
	Bz	4.62	-3.00	-2.68	-0.466	-2.59
	Tyr55	2.45	-2.86	-4.18	-0.509	-4.48
	Trp185	-1.88	-3.41	-0.0663	-0.0573	-5.37
	Tyr314	1.76	-3.44	-4.96	0.991	-6.45
	Trp52	-6.84	-3.43	-0.748	0.378	-11.0
Sub B	Bz	4.28	-3.07	-1.32	-0.353	-0.11
	Tyr228	2.19	-2.94	-0.531	-0.194	-1.27
	Tyr314	1.98	-3.44	-3.61	0.843	-5.03
	Tyr55	1.80	-3.44	-6.63	1.15	-8.24
	Tyr224	1.89	-3.44	-8.36	1.29	-9.83
	Trp185	-6.37	-3.42	-0.480	0.295	-10.2
Monomer	Bz	4.20	-2.92	-6.12	0.651	-4.61
	Tyr228	3.20	-2.77	-6.32	-0.569	-5.46
	Tyr224	2.30	-2.80	-6.10	-0.574	-6.25
	Tyr314	1.68	-3.44	-5.89	1.08	-7.59
	Tyr55	0.25	-3.46	-6.53	1.16	-9.63
	Trp185	-7.36	-3.43	-0.482	0.297	-11.2

[a] ET rates given by eqns (1) and (4) were decomposed into the EC^w, SQ^w and *GTRAM* terms. The quantities were expressed as means over 5000 snapshots with 1 ps time intervals.

[b] $\ln EC^w$ is the logarithmic electronic coupling term (ps^{-1}), derived from eqn (16).

[c] Explicit form of $\ln SQ^w$, derived from eqn (17).

[d] Explicit form of *GTRAM*, derived from eqn (19).

[e] *GT* is total free energy gap, derived from eqn (18).

[f] Logarithmic rate, derived from eqn (20).